Modern Journal of Statistics
2(2), 57–80
DOI: https://doi.org/10.64389/mjs.2026.02260
https://sphinxsp.org/journal/index.php/mjs

Research article

A New Extended Fréchet Distribution: Properties, Characterizations, Modeling, and Risk Analysis for Medical Data

Haitham M. Yousof[1,*], G.G. Hamedani[2], M. Masoom Ali[3], Magdy Tork[4], Manal A. Abdelrahaman[5], Mohammed R. Alzahrani[6], Hassan Alsuhabi[7], Abdirashid M. Yousuf[8], and Abdisalam Hassan Muse[8]

[1] Department of Statistics, Mathematics and Insurance, Faculty of Commerce, Benha University, Benha 13511, Egypt; haitham.yousof@fcom.bu.edu.eg
[2]Department of Mathematical and Statistical Sciences, Marquette University, USA; gholamhoss.hamedani@marquette.edu
[3]Department of Mathematical Sciences, Ball State University, Muncie, IN, USA; mali@bsu.edu
[4]Department of Accounting, College of Business, King Faisal University, Al-Ahsa 31982, Saudi Arabia; mtork@kfu.edu.sa
[5]Department of Quantitative Methods, college of Business, King Faisal University, Al Ahsa 31982, Saudi Arabia; mabdulrahman@kfu.edu.sa
[6]Departmental of Psychology, Faculty of Education, Umm Al-Qura University; Saudi Arabia; mrzahrani@uqu.edu.sa
[7]Department of Mathematics, Al-Qunfudah University College, Umm Al-Qura University, Mecca, Saudi Arabia; hrsuhabi@uqu.edu.sa
[8]Research and Innovation Center, Amoud University, Borama, Somaliland; gees@amoud.edu.so, abdisalam.hassan@amoud.edu.so
***Correspondence:** haitham.yousof@fcom.bu.edu.eg.

Keywords:
Fréchet Distribution
MOO-P Analysis
Peaks Over a Random Threshold
Risk Analysis
Medical Data
Value-at-Risk

Mathematics Subject Classification:
37J39, 62G08

Important Dates:
Received: 25 December 2025
Revised: 9 May 2026
Accepted: 11 May 2026
Online: 24 May 2026

ABSTRACT

Measures like Value-at-Risk (VaR), Tail Value-at-Risk (TVaR), Mean-of-Order-P (MOO-P), and Peaks Over a Random Threshold VaR (PORT-VaR) are important in risk analysis, particularly when it comes to medical data. In order to better capture extreme occurrences in medical applications, this work presents the Extended Rayleigh-Fréchet (ER-Fr) model, a novel extreme value distribution. We derive and discuss several of their key mathematical and statistical properties that are particularly useful for risk assessment. A comprehensive simulation study is conducted to evaluate the performance of the maximum likelihood estimators under various sample sizes, confirming the model's reliability. The practical utility of the ER-Fr distribution is demonstrated through the analysis of two real medical datasets: one on relief times for arthritic patients and another on survival times of guinea pigs exposed to tuberculosis. The model is compared with several existing Fréchet-type distributions using standard goodness-of-fit criteria, and it consistently outperforms its competitors. Based on this analysis, we provide actionable insights and recommendations for healthcare practitioners and risk analysts. The results highlight the ER-Fr model as a powerful and flexible tool for modeling extreme values and assessing risk in medical studies.

1. Introduction

Due to Hamedani and Maadooliat [1], the Fréchet distribution is frequently used to model the upper tail of disease severity data, which is essential for identifying worst-case scenarios in epidemiological studies. This modeling helps predict severe complications in patients with critical conditions of certain diseases, such as cancer and heart disease. For example, extreme values of disease indicators can be modeled to understand the distribution of very high-risk patients, which can inform personalized treatment strategies. Medical devices or treatments also carry an inherent risk of failure. Consequently, the Fréchet distribution is particularly well-suited for modeling failure times and extreme events, such as treatment breakdowns or device malfunctions, which is critical for reliability analysis in life-sustaining medical technologies like pacemakers and surgical implants. In these high-stakes contexts, the distribution facilitates accurate estimation of extreme failure probabilities and inter-failure durations, underscoring its practical utility across diverse reliability applications (see Kotz and Nadarajah [2]; Harrison and Marden [3]).

The Fréchet distribution is frequently employed in survival and reliability analysis for death rates, particularly when researching extreme occurrences, according to Wang and Hu [4]. It is especially helpful in comprehending the upper quantiles of life expectancy or survival time, which are frequently associated with older patients or those receiving life-extending medications, because it accurately represents tail behavior. The following formula provides the probability density function (PDF) and cumulative distribution function (CDF) of the Fr distribution:

$$g_{\beta,\alpha}(x) = \alpha^{\beta}\beta x^{-(\beta+1)} \exp\left(-\alpha x^{-\beta}\right) | x \geq 0 \tag{1.1}$$

and

$$G_{\beta,\alpha}(x) = \exp\left(-\alpha x^{-\beta}\right), \tag{1.2}$$

respectively, where the parameter $\beta > 0$ is a shape parameter and the parameter $\alpha > 0$ refers to the Fr scale parameter. In this work, we study a flexible model called the extended Rayleigh G (ER-G) family, its CDF can be expressed as

$$F_{\vartheta,\sigma,\varpi}(x) = \left\{1 - \exp\left[\nabla_{\sigma,\varpi}(x)\right]\right\}^{\vartheta} | x \in R, \tag{1.3}$$

where the parameter $\vartheta > 0$ is the shape parameter, and ϖ is a parameters vector of base line model and

$$\nabla_{\sigma,\varpi}(x) = -\sigma[G_{\varpi}(x)/\bar{G}_{\varpi}(x)]^2,$$

where the parameter σ is an additional scale parameter, the two function $\bar{G}_{\varpi}(x)$ and $G_{\varpi}(x)$ refers to the survival function (SF) and the CDF of the base line model. For $\sigma = 1$, the new ER-G family is reduced to the Burr X family. The PDF of the ER-G can be expressed as

$$f_{\vartheta,\sigma,\varpi}(x) = 2\vartheta\sigma g_{\varpi}(x)\frac{G_{\varpi}(x)}{\bar{G}_{\varpi}(x)^3}\exp\left[\nabla_{\sigma,\varpi}(x)\right]\left\{1 - \exp\left[\nabla_{\sigma,\varpi}(x)\right]\right\}^{\vartheta-1}. \tag{1.4}$$

Using (1.2), the CDF and the PDF of the ER-Fr can be derived as

$$F_{\vartheta,\sigma,\beta,\alpha}(x) = \left\{1 - \exp\left[\nabla_{\sigma,\beta,\alpha}(x)\right]\right\}^{\vartheta}, \vartheta, \sigma, \beta, \alpha > 0 \tag{1.5}$$

and

$$f_{\vartheta,\sigma,\beta,\alpha}(x) = 2\vartheta\sigma\alpha\beta x^{-(\beta+1)}\frac{\exp\left[\nabla_{\sigma,\beta,\alpha}(x) - 2\alpha x^{-\beta}\right]}{\{1 - \exp(-\alpha x^{-\beta})\}^3}\left\{1 - \exp\left[\nabla_{\sigma,\beta,\alpha}(x)\right]\right\}^{\vartheta-1}, \tag{1.6}$$

respectively, where

$$\nabla_{\sigma,\beta,\alpha}(x) = -\sigma\left[\exp\left(\alpha x^{-\beta}\right) - 1\right]^{-2}.$$

For $\sigma = 1$, the new ER-Fr model reduces to the Burr X Fréchet (BX-Fr) model of Jahanshahi et al. [5]. The term $\nabla_{\sigma,\beta,\alpha}(x)$ tends to 0 as $x \to \infty$, since $\exp\left(\alpha x^{-\beta}\right) \to 1$.

Similarly, $\left[1 - \exp\left(\nabla_{\sigma,\beta,\alpha}(x)\right)\right]^{\vartheta-1}$ will asymptotically behave as a constant since $\nabla_{\sigma,\beta,\alpha}(x)$ tends to 0. Then,

$$f_{\vartheta,\sigma,\beta,\alpha}(x) \sim C x^{\beta-1}.$$

The tail index (TIx), say γ, can be determined by the power-law behavior of our new PDF. Our PDF decays as $x^{\gamma-1}$ for large values of x, so from the obtained expression $x^{\beta-1}$, we have

$\gamma = 1 - \beta$,

which is the TIx of the ER-Fr model.

Recent years have witnessed growing interest in extreme value theory and its applications across medicine, engineering, and

risk management, spurring numerous methodological advances. Notable contributions include Korkmaz et al. [6] on Fréchet computational aspects, Haq et al. [7] on a flexible Fréchet extension for heavy-tailed data, and Yousof et al. [8] on an extreme value framework integrating regression for auxiliary variable assessment, each demonstrating robustness and practical utility in real medical and environmental applications, Chakraborty et al. [9] proposed a new statistical model designed to improve the fit to heavy-tailed data, showing better performance in dealing with positively skewed distributions compared to traditional models such as the generalized extreme value distribution. Its applications in hydrological and financial data have shown significant improvements in tail risk modeling. Jahanshahi et al. [5] introduced the Burr-type Fréchet distribution, a hybrid model that combines the features of Burr and Fréchet distributions to model extreme values, and this model has proven effective in analyzing extreme data in hydrological and insurance risk contexts, focusing on classical and Bayesian inference techniques for parameter estimation.

Elgohari and Yousof [10] also developed a new model that combines copula functions to address multivariate extreme value problems, providing a powerful framework for modeling the dependency structure between correlated extreme events, especially in the fields of finance and environmental risk analysis. Almazah et al. [11] presented a model that uses an asymmetric probability function to account for the skewness of extreme values, which is useful in the scenarios involving extreme events such as natural disasters or stock market crashes. Their model reflects the skewed nature of extreme risks in these applications. Yousof et al. [12] proposed an inverse extension of the Weibull distribution to model extreme values, which is particularly suitable for insurance data, where this model outperformed traditional models in estimating tail risks, providing a more accurate representation of the extreme claims. Finally, Minkah et al. [13] developed a robust model for estimating extreme quanta for Pareto-type tails using an exponential regression framework, and their method has proven effective in assessing risk in areas such as finance and insurance, where extreme events occur rarely but have large impacts.

The expanded Gompertz model was introduced by Alizadeh et al. [14] and demonstrated significant promise in extreme event analysis in reliability and risk analysis when applied to extreme pressure data using the average order P for statistical threshold risk analysis. Ibrahim et al. [15], Yousof et al. [16], Ahmed and Yousof [17], Yousof et al. [18], Yousof et al. [19], Yousof et al. [20], Yousof et al. [21], Afify et al. [22], Elsayed and Yousof [23], Salah et al. [24], Al-babtain et al. [25] and Al-babtain et al. [26].

If $\left|\frac{\xi_1}{\xi_2}\right| < 1$ and $\xi_3 > 0$ then

$$\left(1-\frac{\xi_1}{\xi_2}\right)^{\xi_3-1} = \sum_{w=0}^{+\infty} \left(\frac{\xi_1}{\xi_2}\right)^{w} \frac{(-1)^{w}\Gamma(\xi_3)}{w!\,\Gamma(\xi_3-w)}. \tag{1.7}$$

Apply (1.7) to last term $\{1-\exp[\nabla_{\sigma,\beta,\alpha}(x)]\}^{\vartheta-1}$ in (1.6) we get

$$f_{\vartheta,\sigma,\beta,\alpha}(x) = 2\vartheta\sigma\alpha^{\beta}\beta x^{-(\beta+1)} \frac{\exp(-2\alpha x^{-\beta})}{[1-\exp(-\alpha x^{-\beta})]^{3}} \sum_{w}^{+\infty} \exp[(w+1)\nabla_{\sigma,\beta,\alpha}(x)]. \tag{1.8}$$

Using (1.7) and $A(x; w|\sigma,\beta,\alpha)$, where

$$A(x; w|\sigma,\beta,\alpha) = \exp\left((w+1)\nabla_{\sigma,\beta,\alpha}(x)\right).$$

Then, Equation (1.8) becomes

$$f_{\vartheta,\sigma,\beta,\alpha}(x) \tag{1.9}$$
$$= 2\vartheta\alpha^{\beta}\beta x^{-(\beta+1)} \exp(-2x^{-\beta}) \sum_{w,\varsigma=0}^{+\infty} \frac{(-1)^{w+\varsigma}[\sigma(w+1)]^{\varsigma}\Gamma(\vartheta)}{w!\,\varsigma!\,\Gamma(\vartheta-w)} \frac{\exp[-\alpha(2\varsigma+1)x^{-\beta}]}{[1-\exp(-\alpha x^{-\beta})]^{2\varsigma+3}}.$$

Consider the series expansion

$$\left(1-\frac{\xi_1}{\xi_2}\right)^{-\xi_3} = \sum_{\varkappa=0}^{+\infty} \left(\frac{\xi_1}{\xi_2}\right)^{\varkappa} \frac{\Gamma(\xi_3+\varkappa)}{\varkappa!\,\Gamma(\xi_3)}, \ \left|\frac{\xi_1}{\xi_2}\right| < 1, \ \xi_3 > 0. \tag{1.10}$$

Applying the expansion in (1.10) to (1.9) for the term $B(x; \varsigma|\beta,\alpha)$, where

$B(x; \varsigma|\beta,\alpha) = \{1-\exp[-\alpha x^{-\beta}]\}^{2\varsigma+3}$,

Equation (1.9) becomes

$$f_{\vartheta,\sigma,\beta,\alpha}(x) = \sum_{\varsigma,\varkappa=0}^{+\infty} \epsilon_{\varsigma,\varkappa}\, h_{2\varsigma+\varkappa+2}(x), \tag{1.11}$$

where

$$\epsilon_{\varsigma,\varkappa} = 2\vartheta \frac{(-1)^{\varsigma}\Gamma(\vartheta)\Gamma(2\varsigma+\varkappa+3)}{\varsigma!\,\varkappa!\,\Gamma(2\varsigma+3)(2\varsigma+\varkappa+2)} \sum_{\varpi=0}^{+\infty} \frac{(-1)^{\varpi}[\sigma(\varpi+1)]^{\varsigma}}{\varpi!\,\Gamma(\vartheta-\varpi)},$$

And the density $h_{2\varsigma+\varkappa+2}(x)$ is the Fr model but with shape parameter β and scale parameter $\alpha(2\varsigma+\varkappa+2)^{\frac{1}{\beta}}$. Then, our new CDF of X can be simplified as

$$F_{\vartheta,\sigma,\beta,\alpha}(x) = \sum_{\varsigma,\varkappa}^{+\infty} \epsilon_{\varsigma,\varkappa}\; H_{2\varsigma+\varkappa+2}(x), \tag{1.12}$$

where the function $H_{2\varsigma+\varkappa+2}(x)$ is the Fr CDF. The density graphs show that the ER-Fr distribution can have a single peak and be both symmetric PDF and skewed PDF to the right. This function can be upside-down bathtub HRF, J-shape HRF, growing HRF, decreasing HRF, and increasing-constant-increasing HRF, according to the plots of the ER-Fr HRF for different parameter values shown in Figure 1 (right).

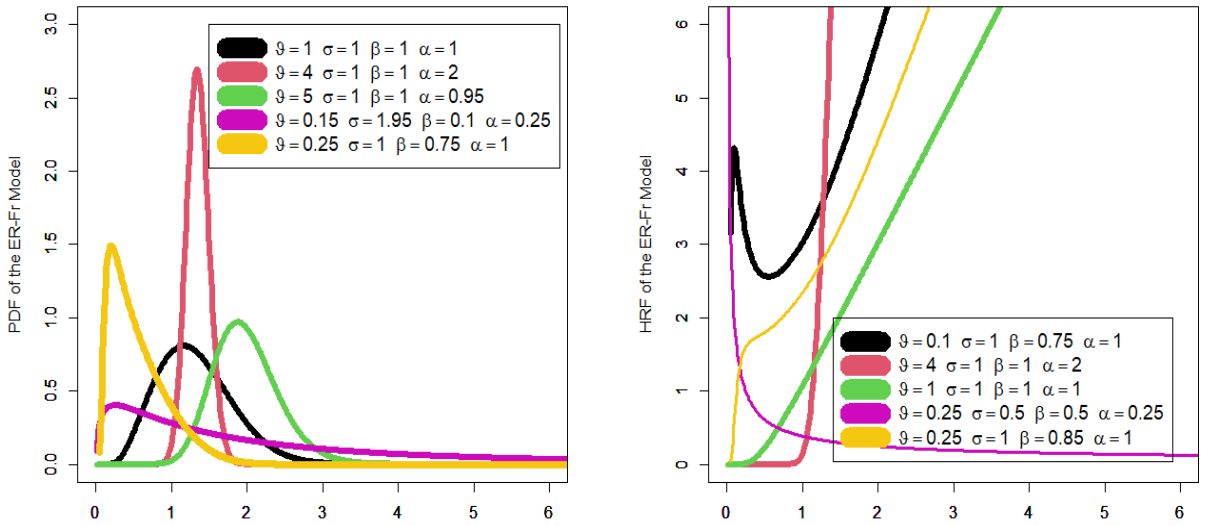

Figure 1: PDF plot (left) and HRF plots (right).

2. Properties

The r^{th} ordinary moment of X is

$$\mu'_r(X) = E(X^r) = \sum_{\varsigma,\varkappa=0}^{+\infty} \epsilon_{\varsigma,\varkappa} \int_{-\infty}^{\infty} x^r h_{2\varsigma+\varkappa+2}(x)\mathrm{d}x$$

Then we obtain

$$\mu'_r(X) = \sum_{\varsigma,\varkappa=0}^{+\infty} \alpha^r\,(2\varsigma+\varkappa+2)^{\frac{r}{\beta}}\Gamma\left(1-\frac{r}{\beta}\right), \forall\, r<\beta, \tag{2.1}$$

The s^{th} incomplete moment (IM), say $I_s(t)$, of X can be expressed from (11), for $r<\beta$, as

$$I_s(X|-\infty,t) = \sum_{\varsigma,\varkappa=0}^{+\infty} \epsilon_{\varsigma,\varkappa} \int_{-\infty}^{t} x^s h_{2\varsigma+\varkappa+2}(x)\mathrm{d}x,$$

which finally can be expressed as

$$I_{\mathcal{S}}(X|-\infty,t)=\sum_{\varsigma,\varkappa=0}^{+\infty}\alpha^{\mathcal{S}}\,\epsilon_{\varsigma,\varkappa}(2\varsigma+\varkappa+2)^{\frac{\mathcal{S}}{\beta}}\Gamma\left(1-\frac{\mathcal{S}}{\beta},\alpha^{\beta}(2\varsigma+\varkappa+2)\left(\frac{1}{t}\right)^{\beta}\right),\forall\,\mathcal{S}<\beta, \qquad (2.2)$$

where

$$\Gamma\left(1-\frac{1}{\beta},\alpha^{\beta}(2\varsigma+\varkappa+2)\left(\frac{1}{x(u)}\right)^{\beta}\right),$$

refers to the lower gamma function.

The general formula for $I_1(t)$ (the first incomplete moment) can be obtained from $I_{\mathcal{S}}(t)$ as

$$I_1(X|-\infty,t)=\sum_{\varsigma,\varkappa=0}^{+\infty}\epsilon_{\varsigma,\varkappa}\,\alpha(2\varsigma+\varkappa+2)^{\frac{1}{\beta}}\Gamma\left(1-\frac{1}{\beta},\alpha^{\beta}(2\varsigma+\varkappa+2)\left(\frac{1}{t}\right)^{\beta}\right).$$

Finally, the quantile function can be obtained as

$$x(u)=\left\{\frac{1}{\alpha}\ln\left[1+\sqrt{\frac{\sigma}{-\ln\left(1-u^{\frac{1}{\vartheta}}\right)}}\right]\right\}^{\frac{1}{\beta}}. \qquad (2.3)$$

where $u\in(0,1)$ represents the probability level.

3. Characterizations

3.1. Characterizations based on a simple relationship between two truncated moments

Using Glänzel's [27] theorem, which holds true even for non-closed intervals or distributions without a closed-form CDF, this subsection describes the ER-Fr distribution by connecting two truncated moments. Moreover, this method provides strong stability under weak convergence, as shown by Glänzel [28], making it a trustworthy instrument for theoretical analysis.

Proposition 3.1.1. If $X:\ \Omega\to(0,\infty)$ is a continuous random variable (RV) and

$$\varrho_1(x)=[P(x)]^{-1},$$

and

$$\varrho_2(x)=\varrho_1(x)\exp\left(-\alpha x^{-\beta}\right)\ \text{ for }\ x>0.$$

If and only if the function $\varkappa(x)$ stated in Theorem 1 takes the form of the following formula, then the RV X has PDF (1.6),

$$\varkappa(x)=\frac{1}{2}\left[1+\exp\left(-\alpha x^{-\beta}\right)\right],\quad x>0,$$

where

$$P(x)=\exp\left(\alpha x^{-\beta}\right)\left[1-\exp\left(-\alpha x^{-\beta}\right)\right]^{-3}\exp\left\{-2\alpha x^{-\beta}-\sigma\left[1-\exp\left(-\alpha x^{-\beta}\right)\right]^{-2}\right\}$$
$$\times\left(1-\exp\left\{-\sigma\left[\exp\left(-\alpha x^{-\beta}\right)-1\right]^{-2}\right\}\right)^{\vartheta-1}.$$

Proof. Let X be a RV with PDF (6) with $C=2\vartheta\sigma\alpha\beta$, then

$$\left(1-F(x)\right)E[\varrho_1(X)\mid X\geq x]=\int_x^{\infty}C\,u^{-\beta-1}\exp\left(-\alpha u^{-\beta}\right)du=\frac{C}{\alpha\beta}\left[1-\exp\left(-\alpha x^{-\beta}\right)\right],\quad x>0,$$

and

$$\left(1-F(x)\right)E[\varrho_2(X)\mid X\geq x]=\int_x^{\infty}Cu^{-\beta-1}\exp\left(-2\alpha u^{-\beta}\right)du=\frac{C}{2\alpha\beta}\left[1-\exp\left(-2\alpha x^{-\beta}\right)\right],\quad x>0,$$

and finally

$$\varkappa(x)\varrho_1(x)-\varrho_2(x)=\frac{\varrho_1(x)}{2}\left[1-\exp\left(-\alpha x^{-\beta}\right)\right]>0,\ \text{ for }\ x>0.$$

Conversely, if $\varkappa$ is given as above, then

$$\mathcal{S}'(x) = \frac{\varkappa'(x)\varrho_1(x)}{\varkappa(x)\varrho_1(x) - \varrho_2(x)} = \frac{\alpha\beta x^{-\beta-1}\exp\left(-\alpha x^{-\beta}\right)}{[1-\exp(-\alpha x^{-\beta})]}, \quad x > 0,$$

and hence

$$\mathcal{S}(x) = -\log\{[1-\exp\left(-\alpha x^{-\beta}\right)]\}, \quad x > 0.$$

Now, in view of Theorem 1, X has density (1.6).

Corollary 3.1.1. Let $X: \Omega \to (0,\infty)$ be a continuous RV and let $\varrho_1(x)$ be as in Proposition 3.1.1. The PDF of X is (1.6) if and only if there exist functions ϱ_2 and $\varkappa$ defined in Theorem 1 satisfying the differential equation

$$\frac{\varkappa'(x)\varrho_1(x)}{\varkappa(x)\varrho_1(x) - \varrho_2(x)} = \frac{\alpha\beta x^{-\beta-1}\exp\left(-\alpha x^{-\beta}\right)}{[1-\exp(-\alpha x^{-\beta})]}, \quad x > 0.$$

Corollary 3.1.2. The general solution of the differential equation in Corollary 3.1.1 is

$$\varkappa(x) = \left[1-\exp\left(-\alpha x^{-\beta}\right)\right]^{-1}\left[-\int \alpha\beta x^{-\beta-1}\exp\left(-\alpha x^{-\beta}\right)\left(\varrho_1(x)\right)^{-1}\varrho_2(x)\mathrm{d}x + \mathrm{D}\right],$$

where D is a constant.

Proof. If X has PDF (1.6), then clearly the differential equation holds. Now, if the differential equation holds, then

$$\varkappa'(x) = \left(\frac{\alpha\beta x^{-\beta-1}\exp\left(-\alpha x^{-\beta}\right)}{[1-\exp(-\alpha x^{-\beta})]}\right)\varkappa(x) - \left(\frac{\alpha\beta x^{-\beta-1}\exp\left(-\alpha x^{-\beta}\right)}{[1-\exp(-\alpha x^{-\beta})]}\right)\left(\varrho_1(x)\right)^{-1}\varrho_2(x),$$

or

$$\varkappa'(x) - \left(\frac{\alpha\beta x^{-\beta-1}\exp\left(-\alpha x^{-\beta}\right)}{[1-\exp(-\alpha x^{-\beta})]}\right)\varkappa(x) = -\left(\frac{\alpha\beta x^{-\beta-1}\exp\left(-\alpha x^{-\beta}\right)}{[1-\exp(-\alpha x^{-\beta})]}\right)\left(\varrho_1(x)\right)^{-1}\varrho_2(x),$$

or

$$\frac{\mathrm{d}}{\mathrm{d}x}\{[1-\exp\left(-\alpha x^{-\beta}\right)]\varkappa(x)\} = -\alpha\beta x^{-\beta-1}\exp\left(-\alpha x^{-\beta}\right)\left(\varrho_1(x)\right)^{-1}\varrho_2(x),$$

from which we arrive at

$$\varkappa(x) = \left[1-\exp\left(-\alpha x^{-\beta}\right)\right]^{-1}\left[-\int \alpha\beta\, x^{-\beta-1}\exp\left(-\alpha x^{-\beta}\right)\left(\varrho_1(x)\right)^{-1}\varrho_2(x)\mathrm{d}x + \mathrm{D}\right].$$

3.2 Characterization in Terms of the Reverse (or Reversed) Hazard Function

The reverse hazard function (RHF), $\mathrm{r_F}$, of a twice differentiable distribution function, F, is defined as

$$\mathrm{r_F}(x) = \frac{\mathrm{f}(x)}{\mathrm{F}(x)}, \quad x \in \text{support of F.}$$

In this subsection we present characterization of LLE distributions in terms of the RHF.

Proposition 3.2.1. If $X: \Omega \to (0,\infty)$ is a continuous RV. The RV X has PDF (6) if and only if its RHF $\mathrm{r_F}(x)$ satisfies the following differential equation

$$\mathrm{r_F'}(x) + (\beta+1)x^{-1}\mathrm{r_F}(x) = \mathrm{C}x^{-\beta-1}\frac{\mathrm{d}}{\mathrm{d}x}\left\{\frac{\left[1-\exp\left(-\alpha x^{-\beta}\right)\right]^{--3}}{1-\exp\{-\sigma[\exp(-\alpha x^{-\beta})-1]^{-2}\}}\right\}, \quad x > 0,$$

with boundary condition $\lim_{x\to\infty}\mathrm{r_F}(x) = 0$.

Proof. Multiplying both sides of the above equation by $x^{\beta+1}$, we have

$$\frac{\mathrm{d}}{\mathrm{d}x}\{x^{\beta+1}\mathrm{r}_{\mathrm{F}}(x)\} = \mathrm{C}\frac{\mathrm{d}}{\mathrm{d}x}\left\{\frac{\left[1-\exp\left(-\alpha x^{-\beta}\right)\right]^{--3}}{1-\exp\{-\sigma[\exp(-\alpha x^{-\beta})-1]^{-2}\}}\right\},$$

or

$$\mathrm{r}_{\mathrm{F}}(x) = \mathrm{C}x^{-\beta-1}\frac{\left[1-\exp\left(-\alpha x^{-\beta}\right)\right]^{--3}}{1-\exp\{-\sigma[\exp(-\alpha x^{-\beta})-1]^{-2}\}},$$

which is the reverse hazard function corresponding to the PDF (1.6).

3.3. Characterization Based on the Conditional Expectation of Certain Function of the RV

Proposition 3.3.1. Let $\mathrm{X} : \Omega \to (\mathrm{e},\mathrm{f})$ be a continuous RV with CDF F. Let $\psi(x)$ be a differentiable function on (e,f) with $\lim_{x\to \mathrm{f}^-}\psi(x) = 1$. Then for $\delta \neq 1$,

$$\mathrm{E}[\psi(\mathrm{X}) \mid \mathrm{X} \leq x] = \delta\psi(x), \quad x \in (\mathrm{e},\mathrm{f})$$

implies

$$\psi_1(x) = \left(\mathrm{F}(x)\right)^{\frac{1}{\delta}-1}. \quad x \in (\mathrm{e},\mathrm{f})$$

Remark 3.3.

For $(\mathrm{e},\mathrm{f}) = (0,1)$, $\psi(x) = 1-\exp\left\{-\sigma\left[\exp\left(-\alpha x^{-\beta}\right)-1\right]^{-2}\right\}$ and $\delta = \frac{\vartheta}{\vartheta+1}$, Proposition 3.3.1 provides a characterization of the ER-Fr distribution (for more details see Hamedani (2013)).

4. Maximum likelihood estimation

Let $x_1, x_2, \ldots, x_{\mathrm{n}}$ be a random sample from our distribution, then the log-likelihood function for Θ, say $\ell = \ell(\Theta)$, can be simplified as

$$\ell = \mathrm{n}\log(2) + \mathrm{n}\log(\vartheta) + \mathrm{n}\log(\sigma) + \mathrm{n}\log\left(\alpha^{\beta}\right) + \mathrm{n}\log(\beta) - (\beta-1)\sum_{w=1}^{\mathrm{n}}\log(x_w)$$
$$+\sum_{w=1}^{\mathrm{n}}\left[-2\alpha^{\beta}\left(\frac{1}{x_w}\right)^{\beta} - \sigma\left(\frac{\mathrm{V}_w}{1-\mathrm{V}_w}\right)^{2}\right] - 3\sum_{w=1}^{\mathrm{n}}\log(1-\mathrm{z}_w)$$
$$+(-1+\vartheta)\sum_{w=1}^{\mathrm{n}}\log\left\{1-\exp\left[-\sigma\left(\frac{1}{\mathrm{V}_w}-1\right)^{-2}\right]\right\},$$

where $\mathrm{V}_w = \exp\left[-{x_w}^{\beta}\alpha^{\beta}\right]$. The last Euation can be easily maximized using the numerical methods. This context, we ignore more details since they are already available in the literature.

5. Performance of MLEs

In this section, we conduct a comprehensive graphical simulation study using R software to evaluate the performance of maximum likelihood estimators (MLEs). The graphical simulation results are presented for various sample sizes to provide more accurate and comprehensive results. For the ER-Fr distribution, the inversion method is particularly effective. The steps to simulate the RV X are as follows:

1. Set n and $\boldsymbol{\Theta}$=($\vartheta, \sigma, \beta, \alpha$).
2. Simulate $u \sim U(0,1)$.
3. Generate x using the inverse CDF method from Equation (1.6).

Repeat these steps n times to obtain $x_1, x_2, \ldots, x_{\mathrm{n}}$ from the ER-Fr distribution with parameters $(\vartheta, \sigma, \beta, \alpha)$.

We used the parameter values $\vartheta = 2$, $\sigma = 1$, $\alpha = 1$ and $\beta = 0.5$, we generated samples of sizes n=50, ..., 450, and 500 from the ER-Fr distribution. The left graph of 1st row of Figure 2 is allocated the bias of $\vartheta|\mathrm{n} = 50, \ldots, 500$. The line plot indicates how the bias changes as the sample size increases. A flatter line closer to zero suggests smaller bias, which indicates that the

estimator for ϑ is becoming more accurate as the sample size grows. The right graph of 1st row of Figure 2 is allocated the MSE of $\vartheta|n = 50, \ldots, 500$. MSE measures the variance and bias of the estimator; thus, a downward trend with increasing n would indicate that the estimator is improving with more data. A consistently low MSE is ideal. The left graph of 2nd row of Figure 2 is allocated the bias of $\sigma|n = 50, 100, \ldots, 500$. The right graph of 2nd row of Figure 2 is allocated the MSE of $\sigma|n = 50, 100, \ldots, 500$. The left graph of 3rd row of Figure 2 is allocated the bias of $\alpha|n = 50, 100, \ldots, 500$. The right graph of 3rd row of Figure 2 is allocated the MSE of $\alpha|n = 50, 100, \ldots, 500$. The left graph of 4th row of Figure 2 is allocated the bias of $\beta|n = 50, 100, \ldots, 500$. The right graph of 4th row of Figure 2 is allocated the MSE of $\beta|n = 50, 100, \ldots, 500$. As sample size increases (shown along the x-axis of each plot), both the bias and MSE decrease for all parameters $(\vartheta, \sigma, \beta, \alpha)$. These plots provide a clear indication that with larger sample sizes, the maximum likelihood estimation procedure becomes more reliable, as both bias and MSE reduce.

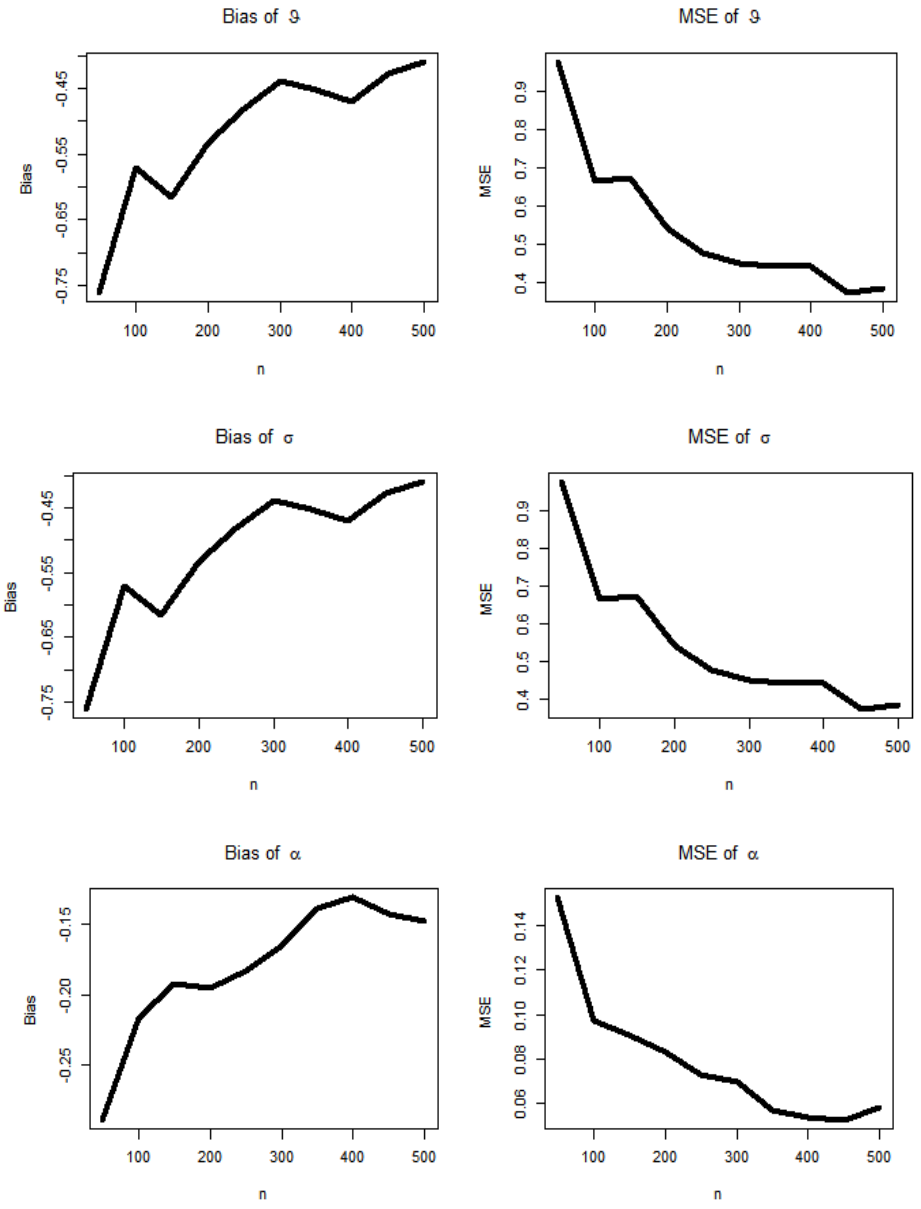

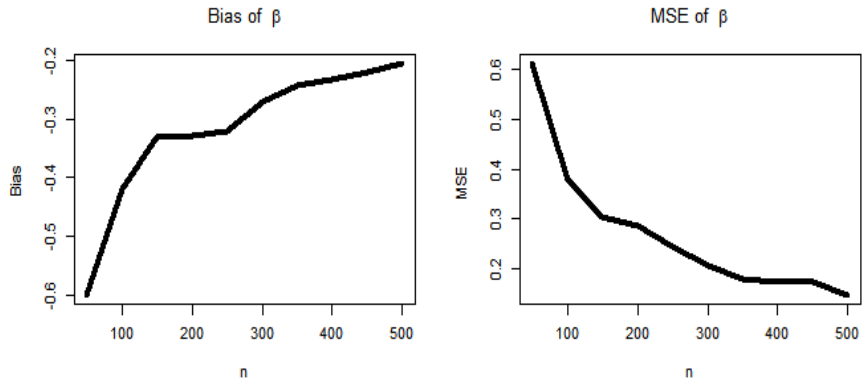

Figure 2: The simulation results.

6. Real data modelling

In order to highlight the significance of the extended Rayleigh-Fr distribution (ER-Fr), which was described in Section 1, we provide two detailed real-world examples in this section. By examining three actual datasets, we show how adaptable this new distribution is.

The fit of the ER-Fr distribution is compared with other models such as the Fr distribution, the Kumaraswamy-Fr distribution (K-Fr), the elevated Fr distribution (E-Fr), the Beta-Fr distribution (B-Fr), the transposed Fr distribution (TR-Fr), the Marshall-Olkin-Fr distribution (MO-Fr), and the McDonald-Fr distribution (Mc-Fr). These comparisons show how the ER-Fr distribution can adapt to different data characteristics, enhancing our understanding of how to handle complex data. By using real-world datasets, we can demonstrate the effectiveness of the new model in representing data more accurately than traditional models, highlighting the strengths of the ER-Fr distribution and enhancing its value in practical applications.

The 1st data set, known as the Wingo data, originates from a clinical trial described by Wingo [29], which investigated relief time (in hours) for 50 arthritic patients. Each patient was subjected to a specific treatment, and the recorded data reflected the time taken for each patient to experience relief from arthritic pain. The relief times were measured in hours and present a range of variability among the patients' responses to the treatment. The data set includes 50 observations, representing the relief times for 50 patients. The relief times range from 0.29 hours to 0.87 hours. In clinical trials, such as the one conducted here, relief time is an important measure of treatment effectiveness. Shorter relief times are usually preferred, as they indicate faster pain relief. The data can be used to assess central tendency as well as variability in treatment effectiveness. The second data set, provided by Bjerkedal [30], includes 72 survival times of rats injected with different doses of tuberculosis. These data represent the number of days that the rats lived after injections and provide valuable insights into the effect of varying doses of tuberculosis on survival rates. The data set consists of 72 survival times, reflecting the life span (in days) of rats after receiving different doses. Survival times range from a minimum of 12 days to a maximum of 376 days, with higher survival times (e.g. 341 and 376 days) being considered outliers. The occurrence of these outliers can be explored using outlier theory or other methods to assess their impact on the overall distribution. Stay times in this group are necessary to evaluate the effect of different doses of tuberculosis bacilli on Pigs. In toxicology or biological experiments, survival time serves as an important endpoint for assessing the impact of treatment or exposure to a particular agent. The tail of the survival distribution could be analyzed using extreme value theory, which helps assess the probability of extremely long survival times (like those above 300 days). Measures such as VaR could be used to calculate the potential risk associated with low survival times (for example, the 5% worst-case scenario), which may be of interest in determining dose safety thresholds.

The 1st data set is: 0.70, 0.84, 0.58, 0.50, 0.55, 0.82, 0.59, 0.71, 0.72, 0.61, 0.62, 0.49, 0.54, 0.36, 0.36, 0.71, 0.35, 0.64, 0.84, 0.55, 0.59, 0.29, 0.75, 0.46, 0.46, 0.60, 0.60, 0.36, 0.52, 0.68, 0.80, 0.55, 0.84, 0.34, 0.34, 0.70, 0.49, 0.56, 0.71, 0.61, 0.57, 0.73, 0.75, 0.44, 0.44, 0.81, 0.80, 0.87, 0.29, 0.50. Figure 3 below describes the 1st data. According to Figure 3, it is noted that the kernel density plot provides a smooth estimate of the distribution of the relief times. The shape of the plot suggests that the data may be somewhat symmetric with potential modes around 0.55 and 0.75. There are no extreme outliers, but some variation is observed in the central and tail regions of the data. The box plot gives a clear summary of the data's distribution, showing the median, quartiles, and any potential outliers. From this plot, the data appears to have a relatively narrow interquartile range (IQR), with some mild outliers at the lower end. The median relief time is around 0.60, and there are no

significant extreme values. The QQ plot checks whether the data follows a normal distribution. In this case, the points deviate from the straight line at the extremes, suggesting that the relief time data does not perfectly follow a normal distribution. The tails (especially the lower end) exhibit some deviation, indicating potential skewness or heavier tails. The TTT plot provides a graphical way to assess the reliability or failure rate of the system. In this case, the curve is concave, suggesting that the failure rate is decreasing over time. This is often associated with early failures or "infant mortality" in reliability contexts. The red dashed diagonal line represents a constant failure rate, and the fact that the plot is above the line suggests a decreasing hazard rate over time. Each plot offers complementary insights into the structure and characteristics of the relief time data, providing a comprehensive picture of the distribution and reliability behavior.

The 2nd data set is: 12, 15, 22, 24, 24, 32, 32, 33, 34, 38, 38, 43, 44, 48, 52, 53, 54, 54, 55, 56, 57, 58, 58, 59, 60, 60, 60, 60, 61, 62, 63, 65, 65, 67, 68, 70, 70, 72, 73, 75, 76, 76, 81, 83, 84, 85, 87, 91, 95, 96, 98, 99, 109, 110, 121, 127, 129, 131, 143, 146, 146, 175, 175, 211, 233, 258, 258, 263, 297, 341, 341, 376. Figure 4 describes the 2nd data. Based on Figure 4, it is noted that the kernel plot illustrates the distribution of the data. It shows a multimodal model with peaks around the values of 55 and 145. The density gradually decreases towards the tails, indicating that while there are a few higher values (like 376), the majority of data points are concentrated between 12 and 100. This suggests a skewed distribution with some clustering in the lower range. The box plot summarizes the key statistics of the data set. The median is around 60, and the interquartile range (IQR) indicates that the central 50% of the data is between approximately 54 and 72. The presence of several outliers above the upper whisker (like 146, 175, and 376) suggests that there are extreme values in the dataset, significantly impacting

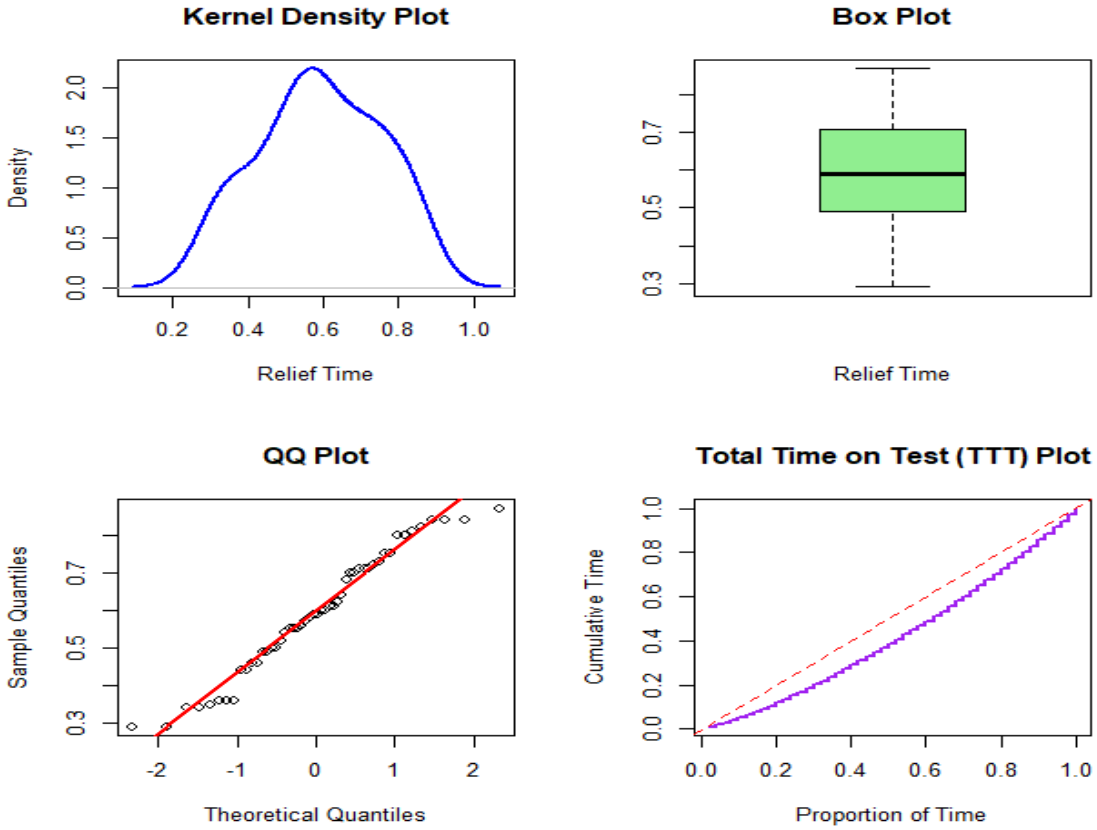

Figure 3: Describing the 1st data.

the overall distribution. The QQ plot compares the quantiles of the data against the quantiles of a normal distribution. The points diverge from the reference line, particularly in the tails, indicating that the data do not follow a normal distribution. The heavy tails and clustering in the middle suggest a right-skewed distribution, potentially indicative of a heavy-tailed behavior. The TTT plot represents cumulative time based on sorted data. The curve shows a consistent increase, suggesting that failures (or events) happen over time, with no indication of early failures. The shape indicates a decreasing hazard rate, which may suggest that items with lower values are likely to fail earlier, while higher values are more robust. Together, these plots provide a comprehensive overview of the dataset's distribution, highlighting its non-normal characteristics and the presence of outliers while indicating reliability trends.

We compute maximum likelihood estimates (MLEs) of the parameters for each model in order to examine and assess the performance of the aforementioned models using three datasets. This guarantees that the parameters are best approximated using the observed data, offering a strong foundation for model comparisons.

In addition to the Anderson-Darling (A*), Cramér-von Mises (W*), and Kolmogorov-Smirnov (K-S) statistics, we assess competing models using the Akaike (AIC) and Bayesian (BIC) information criteria; lower values imply a better match. The ER-Fr distribution's adaptability to various data architectures is successfully highlighted by this multifaceted method, which guarantees a robust selection process that strikes a compromise between model complexity and goodness-of-fit.

In Table 1, we use the AKIC, W*, BIC, A*, K-S, and p-value of the K-S test to assess a number of probabilistic models in light of the relief time data. By decreasing the values of AKIC, W*, BIC, A*, and K-S and maximizing the p-value of the K-S test, the objective is to determine which model best fits the data.

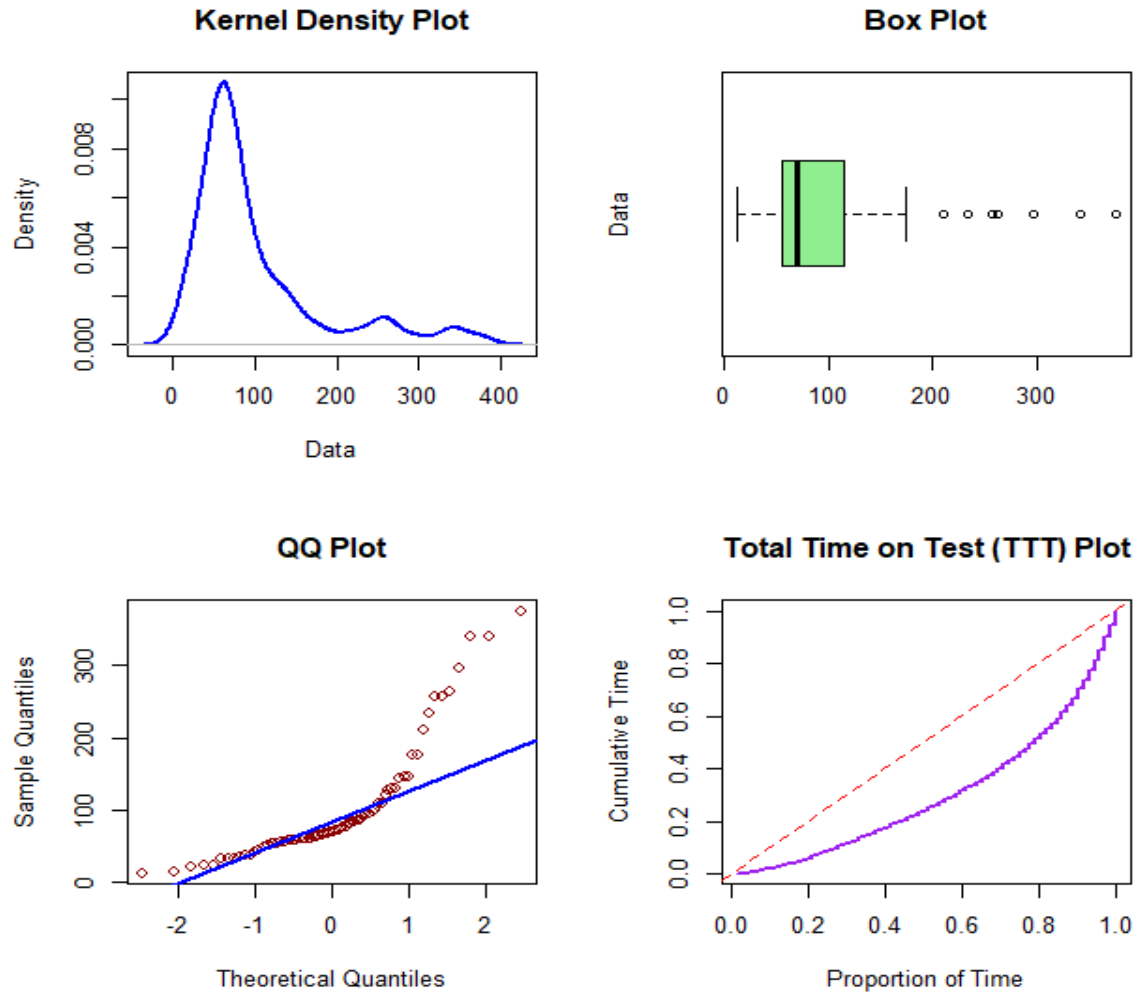

Figure 4: Describing the 2nd data.

When compared to the other models, the ER-Fr model provides the best trade-off between model fit and complexity, as seen by its lowest AKIC (-38.217). Although they are not as good as the ER-Fr, other models such as K-Fr (-32.553) and B-Fr (-34.395) also have competitive AKIC values. Similar to AKIC, the ER-Fr model has the lowest BIC (-30.569), which reinforces its superiority by more severely penalizing complexity than AKIC. B-Fr (-26.747) and K-Fr (-24.905) are the next top models in terms of BIC. With the lowest W* statistic (0.0464), the ER-Fr model has the least overall difference between

the theoretical and empirical distributions. Poorer fits are indicated by the significantly higher W* values (0.3233) of the other models, such as Fr and EFr.

The ER-Fr model also has the lowest A* statistic (0.3654), which means it performs well in capturing tail behavior. Models like Fr (2.0301) and E-Fr (2.0301) have much higher values, indicating less accuracy in fitting extreme data points. The ER-Fr model yields a relatively low K-S statistic (0.0815), indicating a good fit. Other models like K-Fr (0.1053) and B-Fr (0.0981) perform moderately well but are still outperformed by ER-Fr. The ER-Fr model has the highest p-value (0.8937), indicating that the model fits the data well without significant deviations. Lower p-values, such as for the Fr (0.2066) and EFr (0.2064) models, suggest poorer fits, though they are not statistically significant at typical levels. The ER-Fr model consistently outperforms all other models across all metrics, making it the best-fitting model for relief time data. Its low AKIC and BIC values indicate that it balances fitness and complexity efficiently, while its low W*, A*, and K-S values show that it fits both the center and tails of the data well. The high p-value further confirms that the ER-Fr model does not significantly deviate from the empirical distribution. While some models, such as B-Fr and K-Fr, perform moderately well in certain metrics, they do not surpass ER-Fr in overall fit. Models like Fr and E-Fr have notably poor goodness-of-fit statistics, particularly in tail-sensitive measures (W* and A*), which may suggest they are unsuitable for modeling this data set's distribution, especially if capturing extreme values is important.

Finally, Table 2 presents the estimated parameter values and its estimation errors for the relief time data. Table 2 presents the estimated parameters and the corresponding estimation errors for the relief time data across various distributions. The ER-Fr model shows relatively low errors for all parameters, indicating a stable and accurate estimation compared to other models, such as Mc-Fr, which has a high estimation error for ϑ. Other models like Fr and K-Fr exhibit moderate performance, while MO-Fr has the largest errors, suggesting instability in its parameter estimates. Overall, the ER-Fr model demonstrates the best parameter precision.

Table 1: Competitive models under the medical relief times.

Model	AKIC	BIC	A*	W*	K-S	p-value (K-S)
ER-Fr	−38.217	−30.569	0.3654	0.0464	0.0815	0.8937
Fr	−19.701	−15.877	2.0301	0.3233	0.1506	0.2066
K-Fr	−32.553	−24.905	0.5641	0.0680	0.1053	0.6352
E-Fr	−17.701	−11.965	2.0301	0.3233	0.1506	0.2064
B-Fr	−34.395	−26.747	0.4711	0.0557	0.0981	0.7193
TR-Fr	−20.105	−14.369	1.8152	0.2823	0.1370	0.3045
MO-Fr	−29.889	−24.153		0.8560	0.1062	0.6252

Table 2: The estimated parameters and their estimation errors for the relief time data.

	The estimated parameters and its estimation errors.			
Model	σ	ϑ	α	β
Fr	-	-	0.4859	3.2078
	-	-	(0.0227)	(0.3263)
K-Fr	0.29534	122.39	21.470	0.7917
	(0.1881)	(140.51)	(12.846)	(0.1490)
E-Fr	0.9047	-	0.5013	3.2077
	(18.784)	-	(3.2444)	(0.3263)
B-Fr	0.3746	78.718	2.6048	1.2430
	(0.4318)	(48.446)	(4.7654)	(0.6754)
TR-Fr	−0.5816	-	0.4400	3.4974
	(0.2787)	-	(0.0290)	(0.3527)
MO-Fr	52.825	-	0.2897	5.7456
	(96.683)	-	(0.0783)	(0.7440)
ER-Fr	0.0807045	0.3106562	0.5003437	3.1842065
	(0.155261)	(0.118267)	(0.091464)	(0.893496)

The estimated PDFs and associated estimated CDF for the relief time data are shown in Figure 5. The numerical results of Table 1 are confirmed by the results of Figure 5.

Table 3 compares several competitive models based on survival times of guinea pigs injected with different doses of tubercle bacilli, using a range of goodness-of-fit statistics. The models include ER-Fr, Fr, K-Fr, E-Fr, B-Fr, TR-Fr, and Mc-Fr. The B-Fr model has the lowest AKIC (788.592), followed closely by ER-Fr (788.343) and K-Fr (788.666), indicating these three models are among the best fits to the data. Models such as Fr (795.288) and TR-Fr (804.776) have significantly higher AKIC values, suggesting they fit the data less well. The ER-Fr model has the lowest BIC (797.449), indicating that it balances model fit and complexity more effectively than the other models. The TR-Fr model has the highest BIC (815.255), suggesting that it overfits the data compared to the others. The B-Fr model has the lowest W* value (0.13668), indicating a minimal deviation between the theoretical and empirical distribution. The K-Fr (0.14176) and ER-Fr (0.15073) models also perform well on this measure. The TR-Fr model has the highest W* (0.25682), indicating a weaker fit. The B-Fr model has the lowest A* value (0.75314), suggesting it best captures the tails of the data distribution, followed closely by K-Fr (0.77159) and ER-Fr (0.81789).

The TR-Fr model again performs the worst with the highest A* value (1.35866), indicating it poorly fits the extremes of the data. The ER-Fr model has the lowest K-S statistic (0.09663). Other models, such as Fr (0.15188) and TR-Fr (0.18180), have larger K-S values, indicating less accurate fits. With the greatest p-value (0.5121), the ER-Fr model offers the best fit and has the least significant departure from the empirical data. Lower p-values indicate that models such as Fr (0.0721) and TR-Fr (0.0474) are less compatible with the observed data. The model that fits the survival periods of guinea pigs injected with tubercle bacilli the best is the ER-Fr model. With a low AKIC, the lowest BIC, strong W*, A*, and K-S values, and the greatest p-value, it achieves the optimal balance between goodness-of-fit metrics. ER-Fr shines out because of its overall strong fit across all parameters, while B-Fr and K-Fr also perform well. Weaker competitors with subpar results across several areas are models like Fr and TR-Fr.

Table 4 lists the estimated parameter values and their corresponding estimation errors for the survival data. The ER-Fr model stands out with the smallest estimation errors across all parameters, suggesting it provides a precise and stable fit. In contrast, models like Mc-Fr and K-Fr exhibit higher errors for parameters such as ϑ and α, indicating greater uncertainty. Models like Fr and B-Fr show moderate performance, while TR-Fr presents relatively low errors but lacks the same stability seen in the ER-Fr model. Overall, the ER-Fr model offers the most reliable parameter estimates.

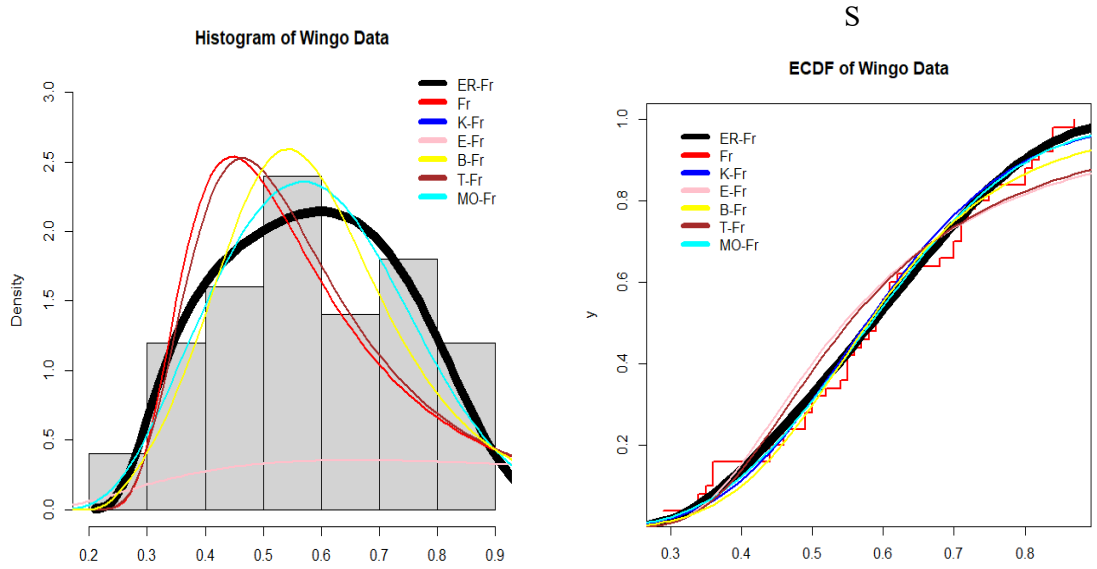

Figure 5: The fitted PDFs and the fitted CDF for the relief time data.

Table 3: Comparing the competitive models under the survival times for guinea pigs that were injected with different doses of tubercle bacilli.

Model	AKIC	BIC	A*	W*	K-S	p-value (K-S)
ER-Fr	788.343	797.449	0.81789	0.15073	0.09663	0.5121
Fr	795.288	799.855	1.28344	0.21477	0.15188	0.0721
K-Fr	788.666	797.777	0.77159	0.14176	0.10568	0.3964
E-Fr	797.293	804.119	1.28292	0.21476	0.15200	0.0716
B-Fr	788.592	797.694	0.75314	0.13668	0.10248	0.4350
TR-Fr	804.776	815.255	1.35866	0.25682	0.18180	0.0474

Table 4: The estimated parameters and their estimation errors for the survival times.

	The estimated parameters and its estimation errors.			
Model	σ	ϑ	α	β
Fr	-	-	54.1999	1.41473
	-	-	(4.7886)	(0.1172)
K-Fr	223.153	5.9443	0.1049	0.7031
	(192.213)	(5.6638)	(0.1323)	(0.2397)
E-Fr	13.01335	-	8.831	1.41465
	(73.1033)	-	(35.086)	(0.1172)
B-Fr	107.372	27.618	0.3143	0.27053
	(40.8406)	(10.153)	(0.3603)	(0.1224)
TR-Fr	−0.71694	-	1.26567	4.71218
	(0.261652)	-	(0.05796)	(0.36570)
ER-Fr	0.0696424	12.73472	0.0335922	0.2513539
	(0.125585)	(11.058758)	(0.044602)	(0.080015)

The calculated PDFs and accompanying estimated CDF for the survival times are shown in Figure 6. Figure 5's findings validate Table 3.

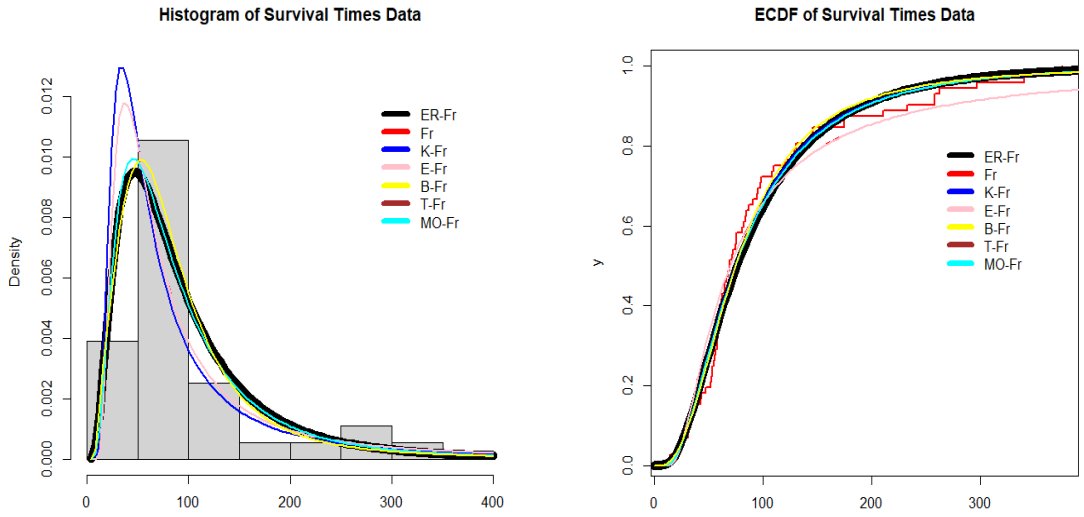

Figure 6: The estimated PDFs and their corresponding estimated CDF for the survival times for guinea pigs that were injected with different doses of tubercle bacilli.

6. Risk analysis for medical data

6.1 The VaR

To compute VAR, we substitute $\mathrm{u} = \varrho$, so

$$\mathrm{VAR}|\varrho = x(\mathrm{u}) = \left\{\frac{1}{\alpha}\ln[1 + \mathrm{T}(\sigma, \vartheta|\varrho)]\right\}^{\frac{1}{\beta}} \tag{6.1}$$

which gives the VaR at the confidence level ϱ, where $\mathrm{T}(\sigma, \vartheta|\varrho) = \sqrt{\sigma/\left[-\ln\left(1-\varrho^{\frac{1}{\vartheta}}\right)\right]}$

6.2 The TVaR

The $\mathrm{TVAR}(\mathrm{X};\Theta)$ of X can be expressed as

$$\mathrm{TVaR}(\mathrm{X};\Theta) = \mathrm{E}(\mathrm{X}|\mathrm{X} > x(\mathrm{u})),$$

which can be derived form

$$\mathrm{TVaR}(\mathrm{X};\Theta) = \frac{1}{1-\mathrm{F}_{\Theta}(x(\mathrm{u}))}\int_{\pi(\varrho)}^{\infty} x\ \mathrm{f}_{\Theta}(x)\,\mathrm{d}x.$$

Then,

$$\mathrm{TVaR}(\mathrm{X};\Theta) = \frac{1}{1-\varrho}\int_{x(\mathrm{u})}^{\infty} x\,\mathrm{f}_{\Theta}(x)\mathrm{d}x.$$

Then,

$$\mathrm{TVaR}(\mathrm{X};\Theta) = \frac{1}{1-\varrho}\sum_{\varsigma,\varkappa}^{+\infty}\epsilon_{\varsigma,\varkappa}\,\alpha(2\varsigma+\varkappa+2)^{\frac{1}{\beta}}\gamma\left(1-\frac{1}{\beta}, \alpha^{\beta}(2\varsigma+\varkappa+2)\left(\frac{1}{x(\mathrm{u})}\right)^{\beta}\right), \tag{6.2}$$

where

$$\gamma\left(1-\frac{1}{\beta}, \alpha^{\beta}(2\varsigma+\varkappa+2)\left(\frac{1}{x(\mathrm{u})}\right)^{\beta}\right) + \Gamma\left(1-\frac{1}{\beta}, \alpha^{\beta}(2\varsigma+\varkappa+2)\left(\frac{1}{x(\mathrm{u})}\right)^{\beta}\right) = \Gamma\left(1-\frac{1}{\beta}\right),$$

and the function $\gamma\left(1-\frac{1}{\beta}, \alpha^{\beta}(2\varsigma+\varkappa+2)\left(\frac{1}{x(\mathrm{u})}\right)^{\beta}\right)$ refers to the upper gamma function. The mean excess loss function $(\tau(\mathrm{X};\Theta)|\varrho)$ can then be expressed as

$$\tau(\mathrm{X};\Theta)|\varrho = \mathrm{TVaR}(\mathrm{X};\Theta) - \mathrm{VaR}|\varrho$$

We direct the reader to important works by Wirch [31], Tasche [32], and Acerbi and Tasche [33] for a more thorough explanation of these methodological underpinnings. Furthermore, Shrahili et al. [34] offer insightful modern perspectives and extensions pertinent to our investigation.

6.3 MOO-P indicator

The MOO-P is a generalized mean because of Elbatal et al. [35] and Alizadeh et al. [14], where the value of PP modifies the sensitivity to the distribution's tail. MOO-P offers a versatile method for evaluating the behavior of extreme occurrences (such as significant financial losses or infrequent medical treatment failures) in risk analysis, particularly with heavy-tailed distributions.

6.5 The PORT-VaR method

The PORT-VAR is a statistical technique used in risk analysis to estimate extreme risk by focusing on the tail of the loss distribution. This technique is particularly effective in cases where traditional VAR methods may not adequately capture the impact of rare and high-severity events. PORT-VAR is based on the Peaks Over the Threshold (POT) method of theory of the extreme values, which models the distribution of values exceeding a certain threshold and introduces a random threshold to enhance the flexibility and accuracy of risk measurement. Traditional POT models use a fixed threshold and focus on the distribution of values (peaks) that exceed this threshold, with the aim of capturing extreme events in the tail of the distribution. These models are typically used to assess financial risks, natural disasters, or other extreme phenomena. However, PORT-VAR introduces a random threshold instead of a fixed threshold, which provides greater flexibility in risk estimation. The random threshold allows the model to take into account changes in the nature of extreme losses, reflecting the real uncertainty in determining the appropriate threshold for extreme events, which is critical in financial markets whose conditions are

constantly changing. In financial markets, PORT-VaR is used to estimate potential maximum losses on assets, portfolios, or financial institutions, especially during periods of market stress. PORT-VaR helps identify extreme risks, such as catastrophic losses or extraordinary claims, providing a more accurate picture of the likelihood and impact of rare events. Additionally, the method can be applied to operational risk, where unexpected losses resulting from events such as fraud, systemic failures, or natural disasters require careful modeling.

6.5 Numerical illustration

In survival and medical analysis or relief time studies, MOO-P can help in stratifying patients based on their risk profiles. By considering higher-order moments (through larger P values), MOO-P helps in identifying individuals with higher risk of extreme outcomes, facilitating targeted interventions. MOO-P's ability to incorporate the tails of the distribution makes it highly relevant in predicting rare but significant medical events, such as long-term survival or extreme relief times.

This increases its usefulness in fields where forecasting such extreme outcomes is essential for patient care planning, such as chronic disease management. The MOO-P analysis under the relief times data is shown in Table 5. As the value of P rises, so do the MOO-P values in Table 5. For P = 1 and 2, the smallest MOO-P is 0.29; for P = 5, it progressively rises to 0.322.

This progression indicates that as we increase the order P, the estimates tend to adjust, becoming more representative of the data's distribution for larger P values. From 0.09036 (P = 1) to 0.07215 (P = 5), the Mean Squared Error (MSE) steadily drops. This decrease demonstrates that as P rises, the model becomes more accurate and has reduced error rates. Additionally, bias decreases as P increases, going from 0.3006 (P = 1) to 0.2686 (P = 5). This implies that the MOO-P estimates for the relief times data are more accurate since the higher P values produce less biased estimates. The MOO-P analysis for the relief timings data is displayed in Figure 7.

Table 5: MOO-P analysis under the relief times data.

P	1	2	3	4	5
TRM	0.5906				
MOO-P	0.29	0.29	0.3066667	0.315	0.322
Bias	0.3006	0.3006	0.2839333	0.2756	0.2686
MSE	0.09036036	0.09036036	0.08061814	0.07595536	0.07214596

Table 6 presents the MOO-P analysis under the survival times data. The MOO-P value in Table 6 rises from 12.0 (P = 1) to 19.4 (P = 5), showing an upward trend as P increases, like Table 5. This indicates that higher values of P provide different perspectives on the distribution, particularly in capturing the higher moments of the survival times data. There is a significant decrease in MSE as P increases. The MSE drops from 7712.255 for P = 1 to 6467.287 for P = 5, signaling that the accuracy of the predictions improves with larger P values. The steep decline in MSE reflects how MOO-P becomes more effective in reducing prediction errors for survival times. Bias reduces from 87.81944 (P = 1) to 80.41944 (P = 5), showing that higher-order moments (as represented by higher P values) yield estimates that are less biased. Figure 8 presents the MOO-P analysis for survival times data.

Table 6: MOO-P analysis under the survival times data.

P	1	2	3	4	5
TRM	99.81944				
MOO-P	12	13.5	16.33333	18.25	19.4
MSE	7712.255	7451.046	6969.931	6653.574	6467.287
Bias	87.81944	86.31944	83.48611	81.56944	80.41944

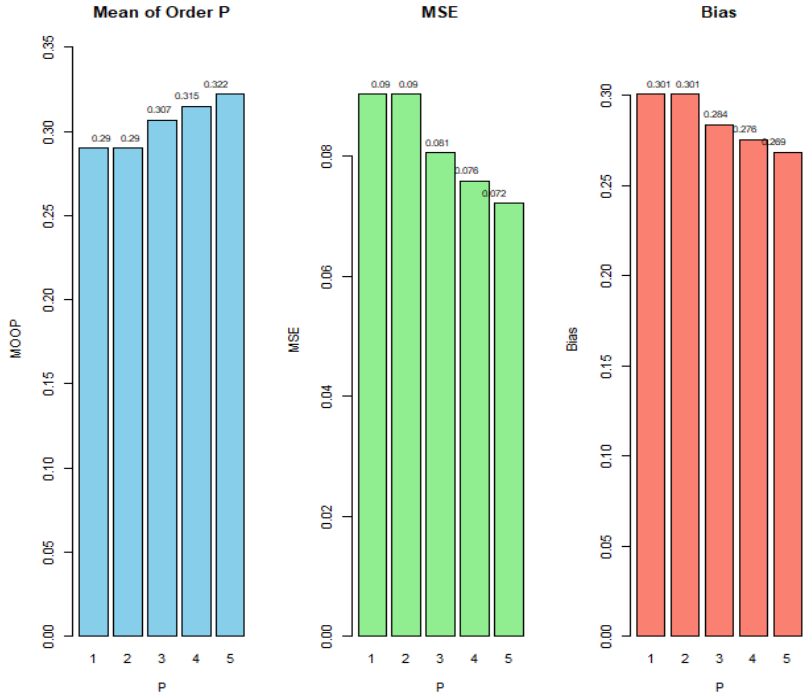

Figure 7: MOO-P analysis for relief times data.

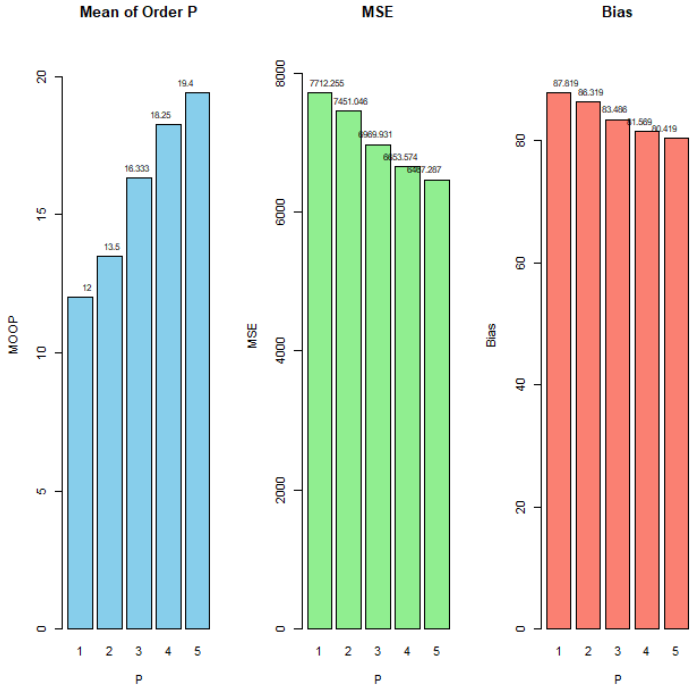

Figure 8: MOO-P analysis for survival times data.

A PORT-VaR study based on medical relief times data at different CL from 55% to 95% is shown in Table 7. The VaR, which is the value at the corresponding confidence level below which the specified percentage of relief times lies, is highlighted in the table. For instance, the VaR is 0.5705 at a 55% confidence level, indicating that 55% of the relief times fall below this figure. Additionally, the number of data points (or "peaks") that surpass the VaR threshold is indicated by the number of Peaks (N. Peaks). The VaR threshold decreases as the confidence level rises, producing more peaks (i.e., more extreme relief times being caught).

Lastly, the summary statistics (minimum peak, first quartile of peaks, median of peaks, mean of peaks, third quartile of peaks, and maximum peak) for the relief times that surpass the VaR threshold at each confidence level are Min., 1st Qu., Median, Mean, 3rd Qu., Max. The distribution of extreme relief times (those that surpass the VaR) at various confidence levels is described by these data. The matching VaR values drop from 0.5705 to 0.3400 when the confidence level increases from 55% to 95%.

This is in line with the hypothesis that more extreme events in the distribution's tail will be captured by greater confidence levels, reducing the threshold. The number of peaks that are above the VaR threshold rises with confidence level. There are 27 peaks at 55% CL and 46 peaks at 95% CL. This is because more data points are captured as peaks as the VAR threshold is lowered (as CL increases). At all confidence levels, the peak's maximum value stays at 0.8700. This suggests that regardless of how the confidence level varies, the most extreme relief time stays constant.

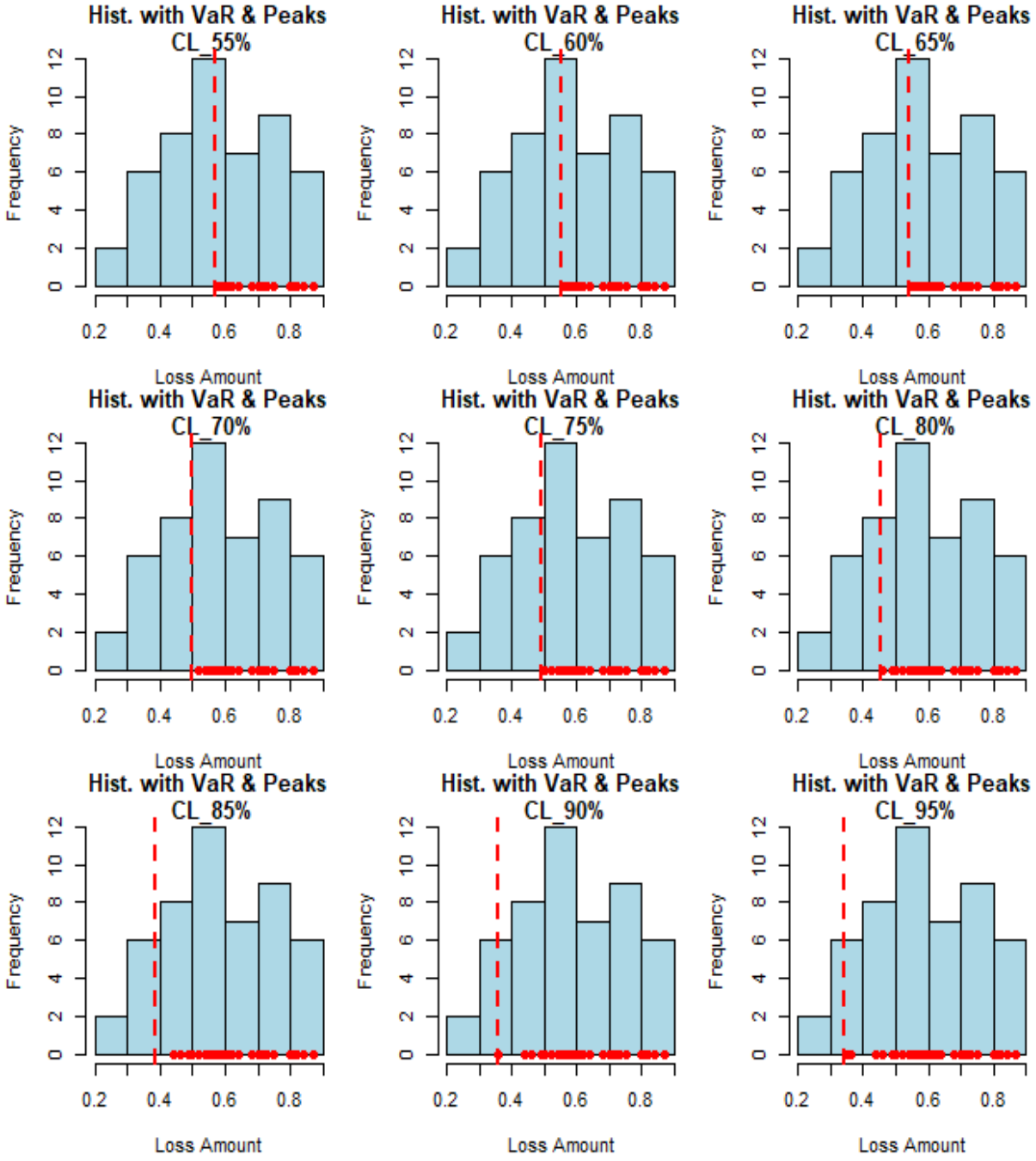

Figure 9: Histograms with VaR and peaks under the relief time.

In the context of medical relief times, the PORT-VaR analysis helps identify extreme relief times, which could represent unusually long or short relief durations. In healthcare, setting an appropriate threshold is vital for identifying outliers in relief times and addressing potential concerns related to treatment efficacy or patient outcomes. The ability to quantify risk in the form of VAR allows for a more structured approach to healthcare management, particularly when dealing with treatments with highly variable outcomes. Recognizing and understanding extreme relief times helps tailor medical responses to patient needs. Figure 9 presents the histograms with VaR and peaks under the relief time. However, Figure 10 shows the density plots of peaks under the relief time. Figure 11 presents some histograms with VaR and peaks under the survival time. However, Figure 12 provides the density plots of peaks under the survival time.

Table 7: VAR, number of peaks under the medical relief times data.

CL	VAR	N. Peaks	Min.,1st Qu., Med., Mean, 3rd Qu., Max.
55%	0.5705	27	0.5800, 0.6150, 0.7100, 0.7119, 0.8000, 0.8700
60%	0.5500	29	0.5600, 0.6100, 0.7100, 0.7017, 0.8000, 0.8700
65%	0.5415	32	0.5500, 0.5975, 0.7000, 0.6875, 0.7625, 0.8700
70%	0.5000	34	0.5200, 0.5900, 0.6900, 0.6782, 0.7500, 0.8700
75%	0.4900	36	0.5000, 0.5775, 0.6600, 0.6683, 0.7500, 0.8700
80%	0.4560	40	0.4600, 0.550, 0.615, 0.649, 0.735, 0.8700
85%	0.3880	42	0.4400, 0.5500, 0.6100, 0.6390, 0.7275, 0.8700
90%	0.3590	45	0.3600, 0.5200, 0.6000, 0.6204, 0.7200, 0.8700
95%	0.3400	46	0.3500, 0.5050, 0.6000, 0.6146, 0.7175, 0.8700

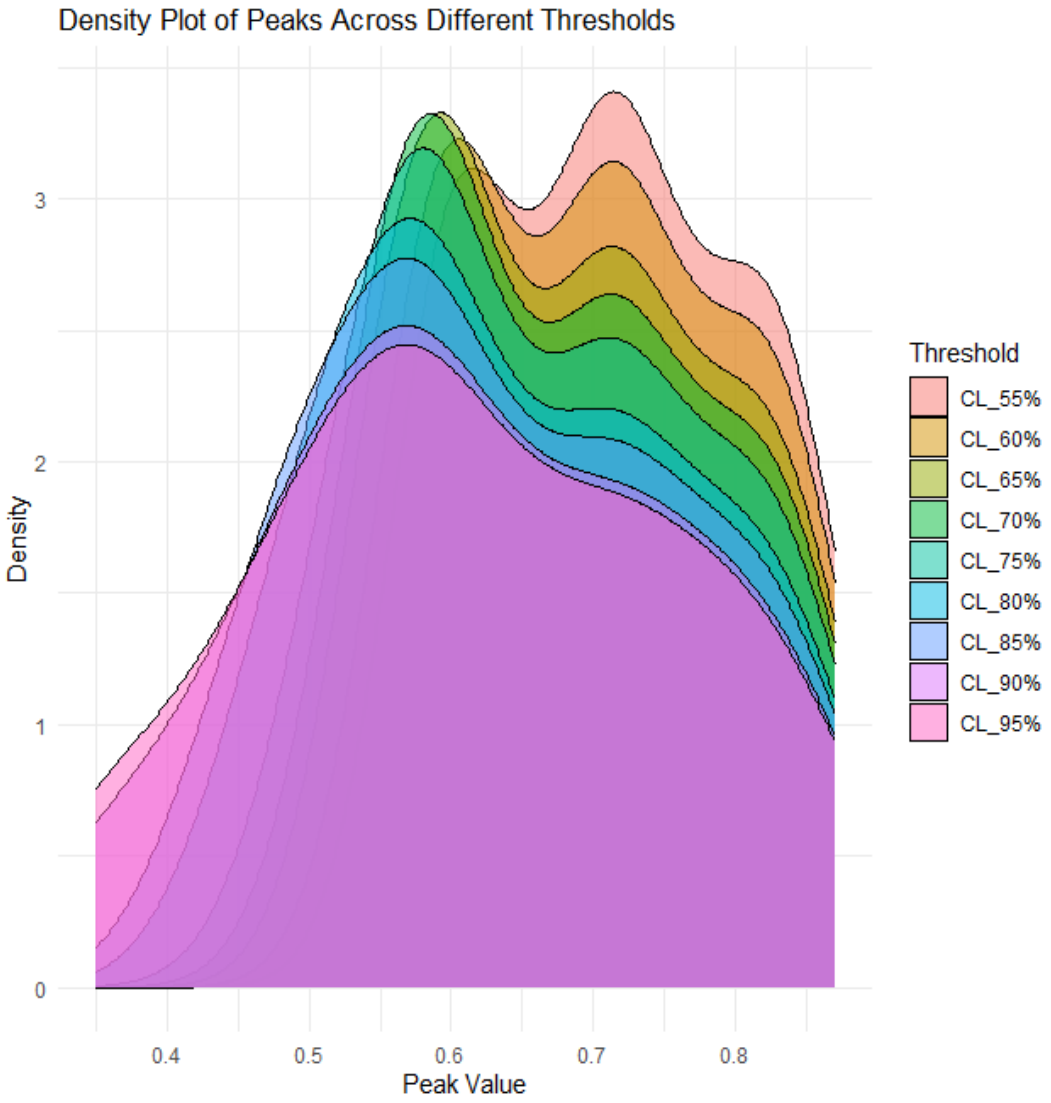

Figure 10: Different density plots of peaks under the relief time.

Table 8 below presents the PORT-VaR analysis of our medical survival times data at various CL from 55% to 95%.

Table 8: VAR, number of peaks under the medical survival times.

CL	VAR	N. Peaks	Min.	1st Qu.	Median	Mean	3rd Qu.	Max.
55%	65.00	39	67.0	82.0	109.0	144.5	175.0	376.0
60%	61.40	43	62.0	75.5	98.0	137.0	160.5	376.0
65%	60.00	44	61.0	74.5	97.0	135.3	153.2	376.0
70%	58.00	49	59.0	70.0	91.0	127.6	146.0	376.0
75%	54.75	54	55.0	65.0	84.5	121.0	140.0	376.0
80%	52.20	57	53.0	62.0	83.0	117.5	131.0	376.0
85%	41.25	61	43.0	60.0	76.0	112.8	129.0	376.0
90%	33.10	64	34.0	59.75	75.50	109.27	127.50	376.0
95%	24.00	67	32.0	58.0	73.0	105.8	124.0	376.0

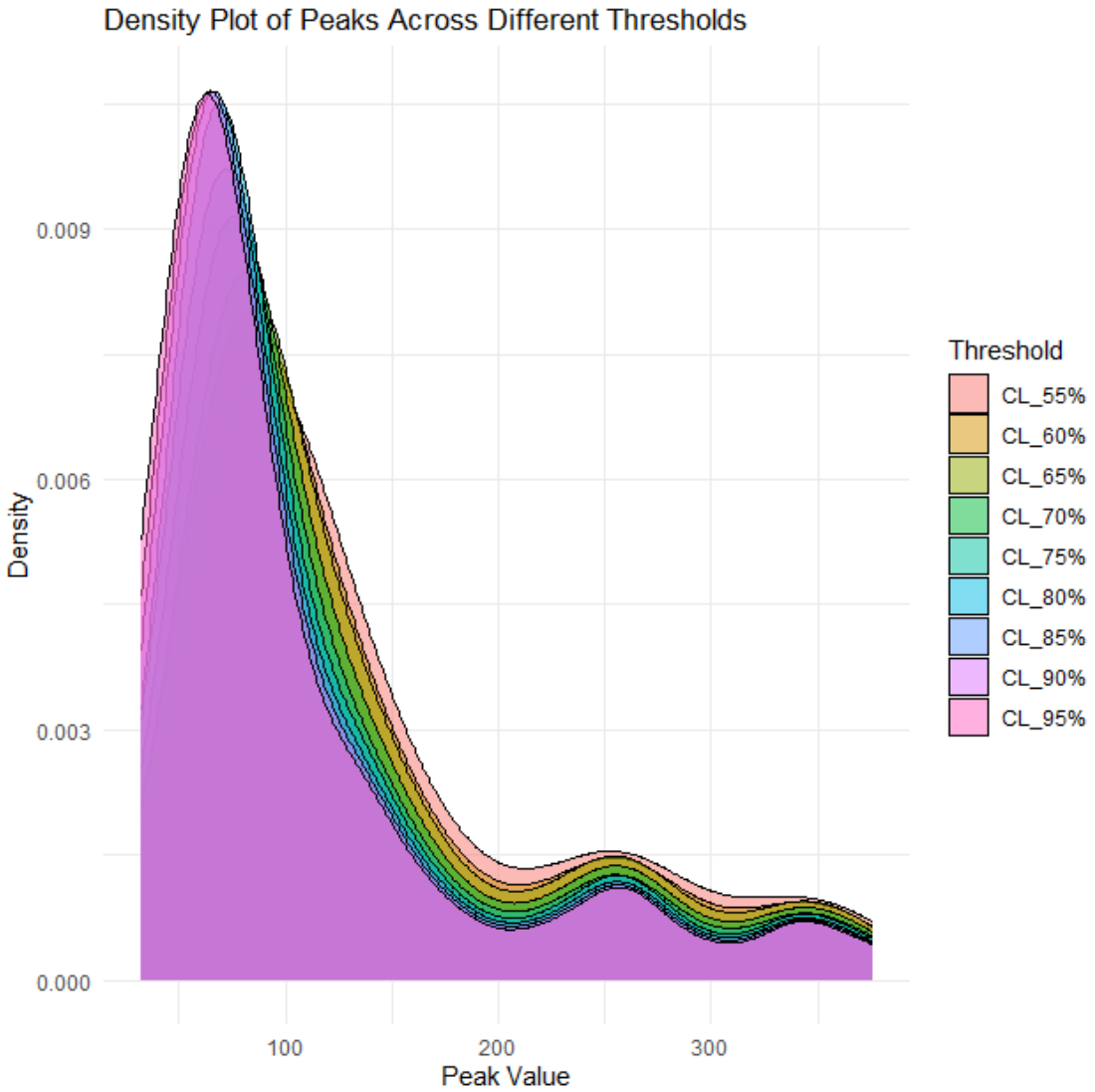

Figure 12: different density plots of peaks under the survival time.

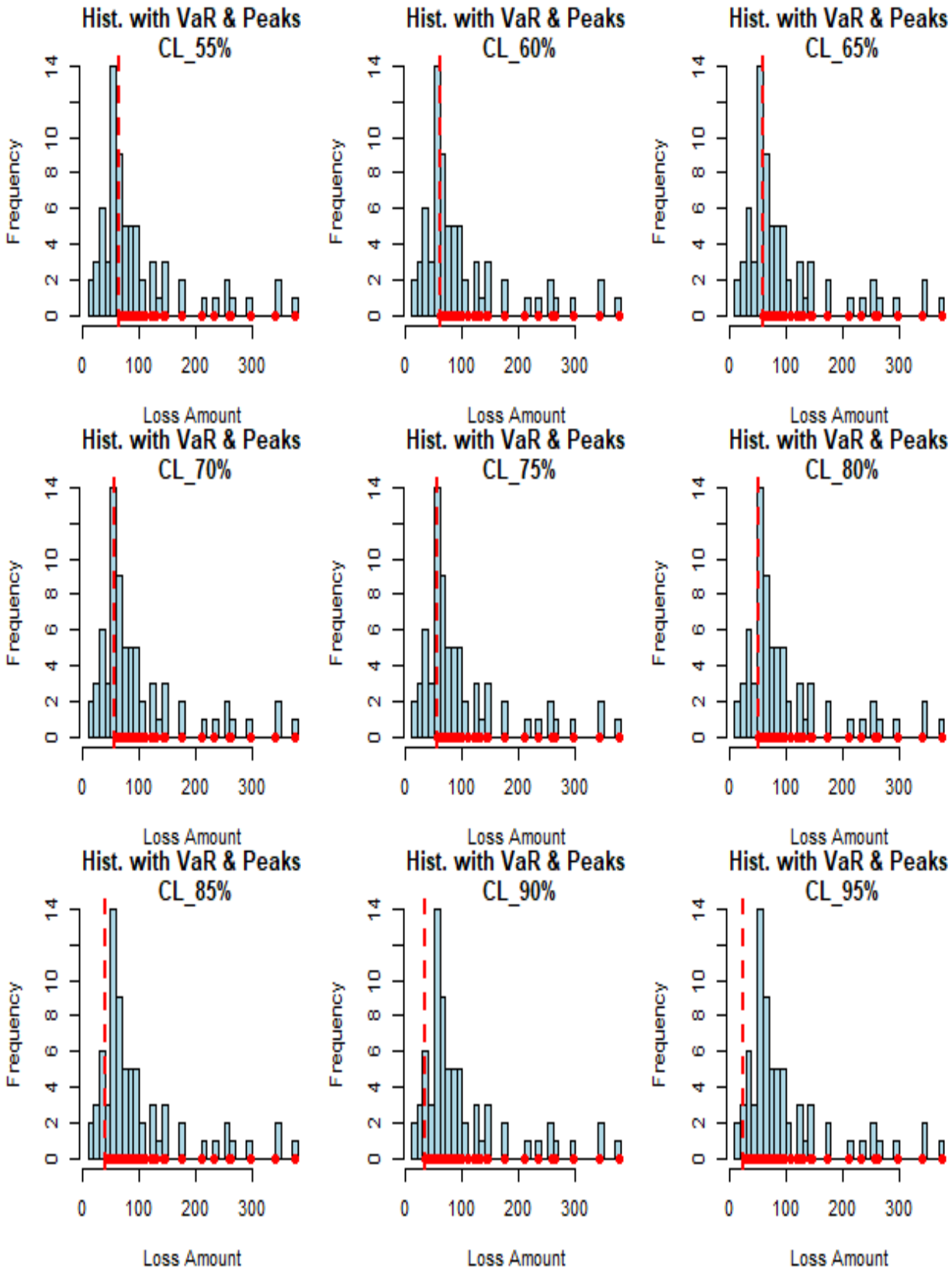

Figure 11: Histograms with VaR and peaks under the survival time.

7. Conclusions

Combining the mean order of P (MOO-P) with the peaks-over a random threshold value at risk (PORT-VaR) in clinical data provides an integrated framework for understanding risk dynamics, enabling healthcare providers to make informed decisions based on normal and extreme patient behaviors. By capturing the nuances of median and extreme survival times, this dual

approach enables the development of more precise and effective treatment strategies, tailored to the individual needs of each patient, enhancing comprehensive patient management. However, the MOO-P provides valuable insights into central trends such as median survival times and their associated variability. These data are essential for understanding the potential effectiveness of treatments within a given population. In contrast, PORT-VaR focuses on identifying thresholds that indicate extreme outcomes, helping patients to identify at high risk, such as predicting serious health problems or adverse events. These thresholds facilitate rapid interventions and efficient allocation of medical resources. This dual framework allows practitioners to monitor and adjust treatments based on data from clinical practice in real time, improving the level of care provided to high-risk groups. This approach is not only effective in improving survival rates, but also in enhancing the quality of life for patients by providing personalized care.

In this paper, we present a new extreme value model known as the extended Rayleigh-Frechet (ER-Fr), which addresses the specific challenges of capturing extreme outcomes in clinical contexts. This model provides a solid mathematical foundation for understanding the distribution of survival times and their direct implications for patient care. A simulation study was performed to validate the effectiveness of this model, using synthetic datasets designed to mimic real-life clinical characteristics, allowing us to test the model's performance in different scenarios. In addition, two real-life datasets were analyzed to compare the new model with other well-known models in the field, helping to highlight the strengths and weaknesses of each. This comparative analysis demonstrated the practical importance of the new model, particularly about the ability to identify anomalies and accurately predict extreme survival times. Ultimately, the combination of MOO-P and PORT-VaR analytics, along with the development of a new extreme value model, represents a major step toward improving medical data analysis. This advance enhances risk assessment and patient management, providing a solid foundation for more sophisticated decision-making in clinical practice. As a result, healthcare providers can improve patient outcomes and ensure high-quality care in a complex healthcare environment, contributing to the overall effectiveness of the healthcare system.

Authors' Contributions:

Conceptualization, H.M.Y. and G.G.H.; Methodology, M.M.A.; Software, M.T.; Validation, M.A.A., M.R.A. and H.A.; Formal Analysis, A.M.Y.; Investigation, A.H.M.; Resources, G.G.H.; Data Curation, G.G.H.; Writing – Original Draft Preparation, H.M.Y.; Writing – Review \& Editing, G.G.H.; Visualization, H.M.Y.; Supervision, H.A.; Project Administration, H.M.Y.; Funding Acquisition, G.G.H.

Data Availability Statement:

The data supporting the findings of this study are available in the article.

Conflicts of Interest:

The authors declare no conflict of interest.

Funding:

This research received no external funding.

References

1. Hamedani, G. G. and Maadooliat, M. (2021). Extreme Value Theory Applications in Medical and Healthcare Studies: A Review. Journal of Statistical Theory and Applications, 20(3), 91–115.
2. Kotz, S., & Nadarajah, S. (2000). Extreme value distributions: theory and applications. world scientific.
3. Harrison, R. L. and Marden, J. I. (2020). The Role of Extreme Value Theory in Modeling Disease Outbreaks: Applications to COVID-19. Journal of Biostatistics, 18(4), 425–440.
4. Wang, S. Y. and Hu, W. L. (2019). Applications of Fréchet Distribution in Medical Device Reliability Analysis. Reliability Engineering & System Safety, 187, 12–23.
5. Jahanshahi, S.M.A., Yousof, H. M. and Sharma, V.K. (2019). The Burr X Fréchet Model for Extreme Values: Mathematical Properties, Classical Inference and Bayesian Analysis. Pak. J. Stat. Oper. Res., 15(3), 797-818.
6. Korkmaz, M. Ç., Yousof, H. M., & Ali, M. M. (2017). Some theoretical and computational aspects of the odd Lindley Fréchet distribution. İstatistikçiler Dergisi: İstatistik ve Aktüerya, 10(2), 129-140.
7. Haq, M. A. ul, Yousof, H. M., & Hashmi, S. (2017). A New Five-Parameter Fréchet Model for Extreme Values. Pakistan Journal of Statistics and Operation Research, 13(3), 617-632.

8. Yousof, H. M., Altun, E., & Hamedani, G. G. (2018a). A new extension of Fréchet distribution with regression models, residual analysis and characterizations. Journal of Data Science, 16(4), 743-770.
9. Chakraborty, S., Handique, L., Altun, E., & Yousof, H. M. (2019). A New Statistical Model for Extreme Values: Properties and Applications. Int. J. Open Problems Compt. Math, 12(1), 97-84.
10. Elgohari, H. and Yousof, H. M. (2021). A New Extreme Value Model with Different Copula, Statistical Properties and Applications. Pakistan Journal of Statistics and Operation Research, 17(4), 1015-1035. https://doi.org/10.18187/pjsor.v17i4.3471
11. Almazah, M.M.A., Almuqrin, M.A., Eliwa, M.S., El-Morshedy, M., Yousof, H.M. (2023). Modeling Extreme Values Utilizing an Asymmetric Probability Function. Symmetry, 2021, 13, 1730. https://doi.org/10.3390/sym13091730
12. Yousof, H.M.; Tashkandy, Y.; Emam, W.; Ali, M.M.; Ibrahim, M. (2023). A New Reciprocal Weibull Extension for Modeling Extreme Values with Risk Analysis under Insurance Data. Mathematics, 2023, 11, 966. https://doi.org/10.3390/ math11040966
13. Minkah, R., de Wet, T., Ghosh, A., & Yousof, H. M. (2023). Robust extreme quantile estimation for Pareto-type tails through an exponential regression model. Communications for Statistical Applications and Methods, 30(6), 531-550.
14. Alizadeh, M., Afshari, M., Contreras-Reyes, J. E., Mazarei, D., & Yousof, H. M. (2024). The Extended Gompertz Model: Applications, Mean of Order P Assessment and Statistical Threshold Risk Analysis Based on Extreme Stresses Data. IEEE Transactions on Reliability, 74(2), 2779-2791. doi: 10.1109/TR.2024.3425278.
15. Ibrahim. M., Handique, L., Chakraborty, S., Butt, N. S. and M. Yousof, H. (2021). A new three-parameter xgamma Fréchet distribution with different methods of estimation and applications. Pakistan Journal of Statistics and Operation Research, 17(1), 291-308. https://doi.org/10.18187/pjsor.v17i1.2887
16. Yousof, H. M., Afify, A. Z., Abd El Hadi, N. E., Hamedani, G. G., & Butt, N. S. (2016). On six-parameter Fréchet distribution: properties and applications. Pakistan Journal of Statistics and Operation Research, 281-299.
17. Ahmed, B., & Yousof, H. (2023). A new group acceptance sampling plans based on percentiles for the Weibull Fréchet model. Statistics, Optimization & Information Computing, 11(2), 409-421.
18. Yousof, H. M., Jahanshahi, S. M. A., Ramires, T. G., Aryal, G. R., & Hamedani, G. G. (2018b). A new distribution for extreme values: regression model, characterizations and applications. Journal of Data Science, 16(4), 677 -706.
19. Yousof, H. M., Rasekhi, M., Altun, E., & Alizadeh, M. (2018c). The extended odd Fréchet family of distributions: properties, applications and regression modeling. International Journal of Applied Mathematics and Statistics, 30(1), 1-30.
20. Yousof, H. M., Butt, N. S., Alotaibi, R. M., Rezk, H., Alomani, G. A., & Ibrahim, M. (2019). A new compound Fréchet distribution for modeling breaking stress and strengths data. Pakistan Journal of Statistics and Operation Research, 15(4), 1017-1035.
21. Yousof, H. M., Hamedani, G. G., & Ibrahim, M. (2020). The Two-parameter Xgamma Fréchet Distribution: Characterizations, Copulas, Mathematical Properties and Different Classical Estimation Methods. Contributions to Mathematics, 2 (2020), 32-41.
22. Afify, A. Z., Yousof, H. M., Cordeiro, G. M., Ortega, E. M., & Nofal, Z. M. (2016). The Weibull Fréchet distribution and its applications. Journal of Applied Statistics, 43(14), 2608-2626.
23. Elsayed, H. A. H., & Yousof, H. M. (2020). The generalized odd generalized exponential Fréchet model: univariate, bivariate and multivariate extensions with properties and applications to the univariate version. Pakistan Journal of Statistics and Operation Research, 529-544.
24. Salah, M. M., El-Morshedy, M., Eliwa, M. S. and Yousof, H. M. (2020). Expanded Fréchet Model: Mathematical Properties, Copula, Different Estimation Methods, Applications and Validation Testing. Mathematics, 8(11), 1949.
25. Al-babtain, A. A., Elbatal, I., & Yousof, H. M. (2020a). A New Flexible Three-Parameter Model: Properties, Clayton Copula, and Modeling Real Data. Symmetry, 12(3), 440.
26. Al-Babtain, A. A., Elbatal, I., & Yousof, H. M. (2020b). A new three parameter Fréchet model with mathematical properties and applications. Journal of Taibah University for Science, 14(1), 265-278.

27. Glänzel, W., A characterization theorem based on truncated moments and its application to some distribution families, Mathematical Statistics and Probability Theory (Bad Tatzmannsdorf, 1986), Vol. B, Reidel, Dordrecht, 1987, 75-84.
28. Glänzel, W., Some consequences of a characterization theorem based on truncated moments, Statistics: A Journal of Theoretical and Applied Statistics, 21 (4), 1990, 613-618.
29. Wingo, D. R. (1983). Maximum likelihood methods for fitting the Burr type XII distribution to life test data. Biometrical journal, 25(1), 77-84.
30. Bjerkedal, T. (1960). Acquisition of Resistance in Guinea Pies infected with Different Doses of Virulent Tubercle Bacilli.
31. Wirch, J. L. (1999). Raising value at risk. North American Actuarial Journal, 3(2), 106-115.
32. Tasche, D. (2002). Expected shortfall and beyond. Journal of Banking & Finance, 26(7), 1519-1533.
33. Acerbi, C., & Tasche, D. (2002). On the coherence of expected shortfall. Journal of banking & finance, 26(7), 1487-1503.
34. Elbatal, I., Diab, L. S., Ghorbal, A. B., Yousof, H. M., Elgarhy, M., & Ali, E. I. (2024). A new losses (revenues) probability model with entropy analysis, applications and case studies for value-at-risk modeling and mean of order-P analysis. AIMS Mathematics, 9(3), 7169-7211.
35. Shrahili, M.; Elbatal, I. and Yousof, H. M. (2021). Asymmetric Density for Risk Claim-Size Data: Prediction and Bimodal Data Applications. Symmetry 2021, 13, 2357. https://doi.org/10.3390/sym13122357